ELSEVIER

Journal of Power Sources 114 (2003) 54–62

JOURNAL OF POWER SOURCES

www.elsevier.com/locate/jpowsour

Modeling of polymer electrolyte membrane fuel cell with metal foam in the flow-field of the bipolar/end plates

Atul Kumar, R.G. Reddy*

Department of Metallurgical and Materials Engineering, The University of Alabama, P.O. Box 870202, Tuscaloosa, AL 35487, USA

Received 16 September 2002; accepted 26 September 2002

Abstract

A unified, three-dimensional, steady-state numerical mass-transfer single cell model for polymer electrolyte membrane fuel cell (PEMFC) was developed. The modeled fuel cell uses metal foam in the flow-field of the bipolar/end plates instead of the conventionally used rectangular channels. Transport equations formulated under the PEMFC conditions were solved using the commercial computational fluid dynamics software Fluent® 6.0 with Gambit® 2.0 as pre-processor. Simulations were performed for different permeability levels of the metal foam in the flow-field. Results showed a significant effect of permeability of the metal foam on the performance of the fuel cell. For example: at 10^{-6} m^2 permeability of metal foam the value of average current density was 5943 A/m^2 while at 10^{-11} m^2 permeability, the average current density was 8325 A/m^2. The average current density value for the multi-parallel flow-field channel design (channel width = 0.0625 in., channel depth = 0.0625 in. and land width = 0.0625 in.), which corresponded to an equivalent permeability value of 4.4×10^{-8} m^2 was 7019 A/m^2. This value for the porous configuration with same permeability and under similar conditions of temperature, pressure and reactants flow rate was slightly lower at 6794 A/m^2. The trend indicated that decreasing the permeability of the flow-field results in better performance from the cell. However, the permeability of the channel design can not be decreased below the value of around 10^{-8} m^2, due to difficulty in machining thinner channels. Consequently, the use of metal foam flow-field is proposed in the bipolar/end plate. The developed model offers fuel cell developers a scope for improvement of the bipolar/end plates in the fuel cell, by switching over to the metal foam flow-field concept.

Keywords: Fuel cells; PEMFC; Bipolar plate; Metal foam; CFD; Fluent

1. Introduction

Fuel cell vehicles (FCVs) may be the only option to meet new EPA emission standards, according to the National Research Council "Review of the Research Program of the Partnership for a New Generation of Vehicles (PNGV) Sixth Report." Despite significant technological progress made with PNGV prototypes unveiled this year (all hybrid AFVs), the report states that production models slated for debut in 2004 will not meet new EPA emission standards [1]. Fuel cell vehicles have the greatest potential to meet these standards and fuel-efficiency requirements. With the launch of *FreedomCAR* (Cooperative Automotive Research) program by US administration in early 2002, the focus is now on mass production and commercialization of hydrogen powered FCVs. The *FreedomCAR* program will focus on development of fuel cell technologies and efficient production of hydrogen from domestic renewable sources. The program replaces the PNGV initiative to make fuel efficient vehicles launched by the US administration in 1993.

It is clear that the fuel cell technology has the right potential to replace the conventionally used internal combustion (IC) engine technology in the automobiles. Among the different types of fuel cells that exist, the polymer electrolyte membrane fuel cell (PEMFC) is seen as a system of choice for automobile applications due to its environmental friendly nature and ability to deliver high power density while operating at lower temperatures [2]. With so much of progress in fuel cell technology in last decade, one of the main hindrances in the onset of fuel cell commercialization program is the high cost of the fuel cell system. The cost of fuel cell stack is currently at US$ 500/kW while the 2004 PNGV goal is US$ 50/kW [3]. Therefore, the main focus for the fuel cell developers is to improve the performance of different components of fuel cell stack by choosing high performance materials and thereby increasing the cell efficiency.

* Corresponding author. Tel.: +1-205-348-1740; fax: +1-205-348-2164.
E-mail address: rreddy@coe.eng.ua.edu (R.G. Reddy).

0378-7753/02/$ – see front matter
PII: S0378-7753(02)00540-2

One such component is the fuel cell bipolar/end plates. These are one of the most important and costliest components of the PEMFC stack and accounts for more than 80% of the total weight of the stack [4]. These plates act as separator plates in between the different cells of the stack, thereby keeping the oxidant and fuel from coming in direct contact. They support intricate gas flow-field patterns that help to direct fuel and oxidant stream to individual cells in the stack. They also act as current collectors and provide a series of electrical connections in between individual cells. The overall efficiency of PEMFC stack depends on the performance of these plates in the fuel cell environment. Although several experiments and model have been developed for the electrochemical process in the fuel cell, these bipolar/end plates have received little attention. The present work focuses on the improvement in the performance of the fuel cell by optimizing the gas flow-field in the bipolar/end plate.

The current design for the flow-field uses the machined rectangular flow channels. Since the flow-field helps to distribute the reactant gases on the surface of the electrode, and remove the by-product water, the dimensions and shape of the channels in the flow-field will affect the performance of the fuel cell. Studies have been done for different channel dimensions, and it was seen that smaller the channel dimensions (channel width, channel depth and land width) and more the number of channels in the flow-field, better is the fuel cell performance [5,6]. For the channel type of flow-field, Kumar and Reddy showed that optimum dimensions exists for the channels that would yield maximum performance from the fuel cell [7]. However, in general, lower is the permeability of the flow-field better would be its performance. The low permeability would result in increased pressure drop across the flow-field. This will make the transfer of reactant gases towards the electrode–membrane reaction interface from diffusion to forced convection type. However, the permeability value of the flow-field can not be decreased beyond 10^{-8} m^2 in case of channel design due to difficulty in machining the thin cross-section channels.

So there is a need to look for alternative technologies which can produce thin cross-section channels, or at least given performance equivalent to that of thin channels. The use of foam materials with an open-porous structure in this regard seems promising. Metal foams are a new kind of material which as on now have not been characterized properly, but do have some alluring properties. They are light and stiff, have good energy absorbing characteristics, and good heat transfer properties. This work therefore focuses on the development of a three-dimensional steady-state numerical mass-transfer model for PEMFC with metal foam in the flow-field of the bipolar/end plates. The model would then be extended for the conventional channel design flow-field. The results obtained from the simulations in both the cases would be studied and compared.

2. Model development

In this research work, a three-dimensional steady-state numerical mass-transfer unified model for PEMFC was developed to predict the cell performance. Numerical predictions of current density as a function of permeability levels of the flow-field would be made. This would help in finding the best permeability values for the metal foams which need to be used in the flow-field. The detailed step-wise development of the model is discussed in following sections.

2.1. Problem domain

The simulation domain consists of two flow-fields with metal foams corresponding to cathode and anode sides separated by membrane electrode assembly (MEA). The MEA consists of anode and cathode porous diffusion layer and catalyst layer, on each side of membrane. The active area of the domain was a square of side 7.62 cm. Fig. 1 shows a detailed view of the model domain (X–Z section), which is composed of a cathode metal foam flow-field, a cathode diffusion layer, a cathode catalyst layer, an anode catalyst layer, an anode diffusion layer, and an anode metal foam flow-field. Each of the layers is marked as separate zone. The diffusion layers were essentially the electrodes made with porous carbon cloth. These layers help to diffuse the reactant gases from the bipolar/end plate flow channels onto the reaction catalyst layer on each sides of the membrane. It was assumed that these layers have an isotropic permeability and the value is 10^{-12} m^2 [8]. The catalyst layer is where all the electrochemical reactions take place. Four species, viz. hydrogen, oxygen, nitrogen, and water vapor were considered in the modeling work. The model works by tracking the fluxes of all the reactants gases along with the by-product water which is formed due to the electrochemical reaction. Consider, for example, the flux for hydrogen species. The hydrogen from the anode flow-field is transported through the anode diffusion layer toward the anode catalyst layer. The catalyst action dissociates the hydrogen molecule to protons and electrons according to the reaction $H_2 \rightarrow 2H^+ + 2e^-$. The protons generated above will transfer through the membrane (protonic conductor) onto the cathode side, wherein they combine with oxygen to generate water. So there is a consumption of hydrogen and oxygen species on the anode and cathode side, respectively, and generation of water species on the cathode side. Similarly other species are tracked in the domain.

2.2. Model assumptions

The following assumptions were used in developing the unified PEMFC model.

(1) Steady-state and stationary conditions exists in the single cell stack. Also, the effect of gravity was neglected.

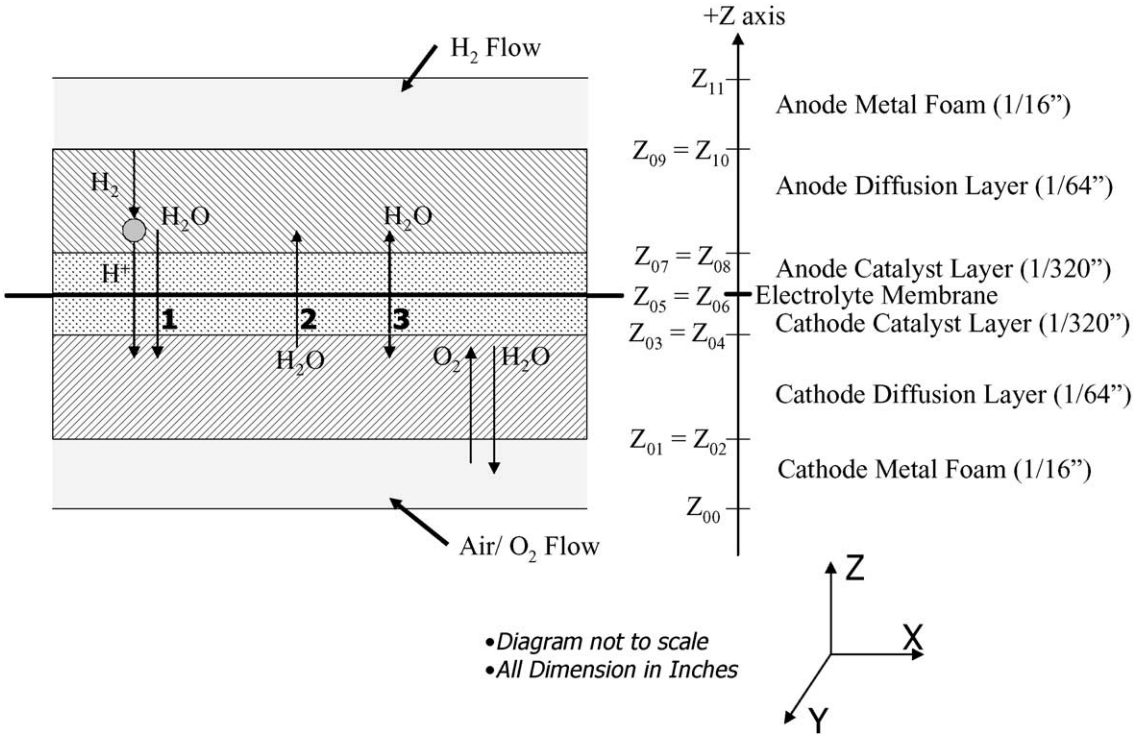

Fig. 1. Schematic of polymer electrolyte membrane fuel cell cross-section showing different zones and species transport across the zones. The net water flux is sum of: (1) electro-osmotic effect, (2) diffusion effect and (3) permeability effect.

(2) Based on the Reynolds number calculation the flow in the fuel cell domain is laminar. Hence, all the transport equations were formulated for laminar behavior.
(3) All the porous zones in the fuel cell domain were assumed to be isotropic.
(4) Four reactant species, viz. H_2, O_2, N_2 and H_2O (vapor) were considered.
(5) The volume of the liquid H_2O was assumed to be negligible in the domain.
(6) Since the density of the gaseous mixture varies from location to location in the domain, compressible gas technique was used to determine the density of the gas mixture.
(7) Gas mixture viscosity was calculated using mass-weighted-mixing-law.
(8) The species binary diffusion coefficient was calculated using kinetic theory of gases.
(9) The oxide film thickness on the bipolar plate was assumed to be constant and that the contact resistance of the bipolar/end plates with the electrodes was a function of compaction pressure of the stack.

2.3. Governing equations

The governing equations for the model can be divided into three different categories, viz. (a) transport equations, (b) thermodynamic equations, and (c) membrane properties equations.

2.3.1. Transport equations

These include equations of continuity, momentum conservation equation, and species transport equations.

2.3.1.1. Equation of continuity. The equations of continuity or mass conservation for steady-state system can be written as

$$\nabla(\rho\vec{v}) = S_{\mathrm{m}} \tag{1}$$

where ρ is the density of the gaseous mixture, $\vec{v}$ the velocity vector, and S_{m} the source term for the continuous phase. The value of S_{m} is zero for all other zones in fuel cell domain, except that in catalyst layer for both anode and cathode sides. The source term in the anode and cathode catalyst layer is given as

$$S_{\mathrm{m,a}} = S_{\mathrm{H_2}} + S_{\mathrm{w,a}} \tag{2}$$

$$S_{\mathrm{m,c}} = S_{\mathrm{O_2}} + S_{\mathrm{w,c}} \tag{3}$$

where the subscripts 'a' and 'c' refer to the anode and cathode side, respectively, and S_{x} (x = H_2, O_2, w (water)) represent the source terms for species x in the catalyst layer. The density (ρ) of the mixture is calculated using the compressible gas technique [9] and is given for multi-component system as

$$\rho = \frac{P_{\mathrm{op}} + P}{RT\sum_i m_i/M_i} \tag{4}$$

where P_{op} is the operating pressure, P the local relative (or gauge) pressure, m_i the mass-fraction of species i, and M_i the molecular weight of species i.

2.3.1.2. Momentum conservation equations. The momentum conservation equations or the Navier–Stokes equations for steady-state system can be described as

$$\nabla(\rho\vec{v}\vec{v} + P) + \vec{S}_p = S_{m,k}\vec{v} \tag{5}$$

where S_p is the momentum source term. For small velocities and transport in porous media, the momentum source term S_p is given by Darcy's Law:

$$\vec{S}_p = -\left(\frac{\mu}{\beta}\right)\vec{v} \tag{6}$$

where μ is the viscosity of the gaseous mixture given by mass-weighted mixing law:

$$\mu = \sum_i m_i\mu_i \tag{7}$$

and β is the permeability of the medium. The value of β was taken to be 10^{-12} m^2 for the electrodes and catalyst layer. The permeability, β for the metal foam flow-field in the bipolar/end plates was varied from 10^{-6} to 10^{-12} m^2.

2.3.1.3. Species transport equations. These are written for each of the species H_2, O_2, N_2, and H_2O (vapor). On the anode side, the species transport equations are

$$\nabla(\rho\vec{v}m_{H_2}) = -\nabla\cdot\vec{J}_{H_2} + S_{H_2} \tag{8}$$

$$\nabla(\rho\vec{v}m_{w,a}) = -\nabla\cdot\vec{J}_{w,a} + S_{w,a} \tag{9}$$

and for the cathode side the species transport equations of O_2, N_2, and H_2O are

$$\nabla(\rho\vec{v}m_{O_2}) = -\nabla\cdot\vec{J}_{O_2} + S_{O_2} \tag{10}$$

$$\nabla(\rho\vec{v}m_{N_2}) = -\nabla\cdot\vec{J}_{N_2} \tag{11}$$

$$\nabla(\rho\vec{v}m_{w,c}) = -\nabla\cdot\vec{J}_{w,c} + S_{w,c} \tag{12}$$

where J_i is the diffusion flux of species i.

The diffusion flux is given by Maxwell relationship [9]:

$$\vec{J}_i = -\sum_{j=1}^{N-1}\rho D_{i,j}\nabla m_j \tag{13}$$

where $D_{i,j}$ is the binary diffusion coefficient of species i in species j, and N the total number of species in the mixture. The binary diffusion coefficients ($D_{i,j}$) were calculated using the kinetic theory of gases as described in Fluent® user manual [9]. The source terms for each of the species transport equations exist only in their respective catalyst layer and are given by

$$S_{H_2} = \left[-\frac{I(x,y)}{2F}\right]M_{H_2}A_{CV} \tag{14}$$

$$S_{w,a} = \left[-\frac{\alpha(x,y)}{F}\right]I(x,y)M_{H_2O}A_{CV} \tag{15}$$

$$S_{O_2} = \left[-\frac{I(x,y)}{4F}\right]M_{O_2}A_{CV} \tag{16}$$

$$S_{w,c} = \left[\frac{1+2\alpha(x,y)}{2F}\right]I(x,y)M_{H_2O}A_{CV} \tag{17}$$

where $I(x, y)$ is the local current density, F the Faradays constant, $\alpha(x, y)$ the local net water transfer coefficient per proton and A_{CV} the specific surface area of control volume element in the domain.

2.3.2. Thermodynamic equations

The various reactions for a PEMFC fed with hydrogen containing anode gas and oxygen containing cathode gas are

$$\text{anodic}: \quad H_2 \rightarrow 2H^+ + 2e^- \tag{18}$$

$$\text{cathodic}: \quad \tfrac{1}{2}O_2 + 2H^+ + 2e^- \rightarrow H_2O \tag{19}$$

$$\text{net reaction}: \quad H_2 + \tfrac{1}{2}O_2 \rightarrow H_2O. \tag{20}$$

The Nernst equation for the H_2/O_2 fuel cell, using literature values of the standard-state entropy can be written as [10]:

$$E = 1.229 - (8.5\times10^{-4})(T - 298.15) + (4.308\times10^{-5})T(\ln(p^*_{H_2}) + \tfrac{1}{2}\ln(p^*_{O_2})) \tag{21}$$

where E (volts) is the ideal equilibrium potential, T (K) the cell temperature and P^*_i (atm) is the partial pressures of species i at the reaction interface. However, due to the irreversible losses in a practical fuel cell the actual cell potential is decreased from its equilibrium potential. These losses include activation polarization (η_{act}), ohmic polarization (η_{ohm}), and concentration polarization (η_{conc}). The actual cell voltage (V) is then, theoretical cell voltage (E) minus the polarization losses.

$$V = E - \eta_{act} - \eta_{ohm} - \eta_{conc}. \tag{22}$$

Activation polarization is present when the rate of an electrochemical reaction at an electrode surface is controlled by sluggish electrode kinetics. The loss arises due to the activation barrier that must be overcome by the reacting species. This is given by the equation [2]:

$$\eta_{act} = \frac{RT}{F}\ln\left(\frac{I(x,y)}{I_o}\right) \tag{23}$$

where I_o is the exchange current density (A/m^2).

The ohmic polarization occurs because of the resistance to flow of electrons in cell components and resistance to the flow of ions in the electrolyte, and is given by [2]:

$$\eta_{ohm} = I(x,y)R_{cell}(x,y) \tag{24}$$

$$R_{cell}(x,y) = R_{CR}(x,y) + R_{memb}(x,y) \tag{25}$$

where $R_{CR}(x, y)$ is the contact resistance of the stack and R_{memb} the resistance offered by the electrolyte membrane to

the flow of H^+ ions. The contact resistance depends upon the type of material for the metal foam in the flow-field of the bipolar/end plate and compaction force of the stack. In this model, SS-316 metal foam was used. A relationship between compaction force and contact resistance for SS-316 was developed by curve fitting the data from Hodgson et al. [11]. The equation for contact resistance for SS-316 is given by:

$$R_{CR}^{SS\text{-}316} = 2.62F_{stk}^{-0.9231} \tag{26}$$

where $R_{CR}^{SS\text{-}316}$ is the contact resistance ($\Omega\,m^2$) and F_{stk} the compaction pressure of the stack in N/m^2. The high contact resistance in case of using metallic components is due to the formation of thin oxide layer on the surface. Hence, these contact losses are considered in our modeling calculations. The resistance to flow of ions (H^+) in the electrolyte membrane depends on the proton conductivity of the membrane (σ_m) and the thickness of the membrane (t_m), and is given by the expression:

$$R_{memb} = \frac{t_m}{\sigma_m(x,y)}. \tag{27}$$

It may be noted that the electrolyte membrane is a conductor of protons (H^+) and is an insulator for the electrons. Consequently only the protons will be passing the electrolyte membrane from the anode to cathode side, while the electrons will follow the outer circuit generating current.

Concentration polarization arises due to the consumption of the reactant gases at the reaction site and the inability of the surrounding material to maintain the initial concentration of the bulk fluid. That is, a concentration gradient is formed. Several processes like slow diffusion of the reactants in the electrode pores, diffusion of the reactants and products to/from the electrochemical reaction site, etc. may contribute to concentration polarization. Concentration polarization is given as a function of limiting current, $I_L(x, y)$ by the following expression [2]:

$$\eta_{conc}(x,y) = \frac{RT}{nF}\ln\left(1 - \frac{I(x,y)}{I_L(x,y)}\right). \tag{28}$$

2.3.3. Membrane properties equations

The water content and the flux of water in the membrane are important for current density prediction in the cell [8,12]. The equations for the electrolyte membrane properties are empirical equations and are obtained by experimental data done by some researchers [8,14,15]. It may be noted that all the properties referred to in this section are the local properties values on the *X–Y* reaction interface, and the suffix (x, y) has been taken out just for mere simplicity. The activity of water (a) on the membrane–electrode interface is given by

$$a_k = \frac{X_{w,k}P}{P_{w,k}^{sat}} \tag{29}$$

where subscript k ('k' = 'a' or 'c') refers to either the anode or cathode side, $X_{w,k}$ is the mole fraction of water at 'k' interface, P the pressure and $P_{w,k}^{sat}$ is the saturation vapor pressure of water at 'k' interface and is given by [13]:

$$\log_{10}(P_{w,k}^{sat}) = 2.95\times10^{-2}T_k - 9.18\times10^{-5}T_k^2 + 1.44\times10^{-7}T_k^3 - 2.18 \tag{30}$$

where $P_{w,k}^{sat}$ is in atm and T_k the temperature at the 'k' interface in °C. The water content (λ) in the membrane is given as a function of the activity of water on anode side by the expression [8]:

$$\lambda = 0.043 + 17.81a_k - 39.85a_k^2 + 36a_k^3, \quad 0 < a_k \le 1 \tag{31a}$$

$$\lambda = 14 + 1.4(a_k - 1), \quad 1 < a_k \le 3. \tag{31b}$$

The proton (H^+), which is a charged particle, attracts the polar water molecule and drags it along with from anode to cathode side. This is called as the electro-osmotic effect. More accurately, it is the hydronium ion $[H^+(H_2O)_n]$ ion which passes through the membrane. The empirical equation describing this effect is [13]

$$n_d = 0.0029\lambda^2 + 0.05\lambda - 3.4\times10^{-19} \tag{32}$$

where n_d is the electro-osmotic drag coefficient. The diffusion coefficient of water (D_w) in the membrane at temperature T_c (K) is given by the expression [13]:

$$D_w = D_i\exp\left(2416\times\left(\frac{1}{T_o} - \frac{1}{T_c}\right)\right), \quad T_o = 303\,K \tag{33}$$

where

$$D_i = 10^{-10}, \quad \lambda < 2$$

$$D_i = 10^{-10}(1 + 2(\lambda - 2)), \quad 2 \le \lambda \le 3$$

$$D_i = 10^{-10}(3 - 1.67(\lambda - 3)), \quad 3 < \lambda < 4.5$$

$$D_i = 1.25\times10^{-10}, \quad \lambda \ge 4.5.$$

The water concentration ($C_{w,k}$) at membrane–electrode interface is given by [8]:

$$C_{w,k} = \frac{\rho_{m,dry}}{M_{m,dry}}(0.043 + 17.8a_k - 39.85a_k^2 + 36a_k^3), \quad a_k \le 1 \tag{34a}$$

$$C_{w,k} = \frac{\rho_{m,dry}}{M_{m,dry}}(14 + 1.4(a_k - 1)), \quad a_k > 1 \tag{34b}$$

where $\rho_{m,dry}$ is the density of dry membrane ($2000\,kg/m^3$ [6]) and $M_{m,dry}$ the equivalent weight of dry membrane (1.1 kg/mol [6]). The local membrane proton conductivity (σ_m) is then given by [13]:

$$\sigma_m = \left(0.514\frac{M_{m,dry}}{\rho_{m,dry}}C_{w,a} - 0.326\right)\times\exp\left[1268\left(\frac{1}{T_o} - \frac{1}{T_a^s}\right)\right], \quad T_o = 303\,K. \tag{35}$$

The net water transfer coefficient (α) in the membrane is given by the expression [14]:

$$\alpha = n_d - \frac{F}{I}\left[D_w \frac{(C_{w,c} - C_{w,a})}{t_m} + C_{w,m}\frac{k_p}{\mu_{H_2O}}\frac{\Delta P_w}{t_m}\right] \quad (36a)$$

where $C_{w,m}$ is the concentration of water in the membrane, k_p the permeability of water in membrane, μ_{H_2O} the viscosity of water. The effect of third term (convection term) in Eq. (36a) is very small [13], and is neglected in this study. The modified expression for net water transfer coefficient (α) in the membrane is then:

$$\alpha = n_d - \frac{F}{I}\left[D_w \frac{C_{w,c} - C_{w,a}}{t_m}\right]. \quad (36b)$$

2.4. Solution strategy

The model equations were solved using the commercial computational fluid dynamics software Fluent® 5.5 using Gambit® 2.0 as a preprocessor [9]. The flow domain consists of a membrane electrode assemble (MEA), and the cathode and anode flow-fields with metal foams. A hexahedron volume element with 20 nodes per element, and *map* scheme was chosen for meshing the domain. Total number of the volume elements with the chosen mesh size was around 0.4 million. The formulated transport equations, viz. continuity, momentum balance, and species flux equations were solved using the *Simple* algorithm [9] for each of the control volume element in the domain. Thermodynamic equations for the electrochemical reactions and equations for membrane properties were incorporated in the source terms with the introduction of user defined functions (UDFs) codes. All the equations were solved and the parameters were updated at the start of every iteration using the *adjust* function. UDFs codes were written in the C language and were passed as an input to the Fluent® software during the post-processing step. Because of the memory and time requirements for solving these equations, the Fluent® and the Gambit® software's were run on Dell® Precision® workstation (Intel® Xeon® 2.2 GHz, 1.5 GB SDRAM).

3. Results and discussion

Simulations were done for different permeability levels of the metal foam flow-field. The permeability of the metal foam was varied from 10^{-6} to 10^{-12} m^2. Simulations were performed at temperature and pressure of 350 K and 202 kPa. Externally humidified reactant gases were used. The anode reactant gas consists of 40 mass% of H_2 and 60 mass% of H_2O vapor. On the cathode side, the reactant gas was humidified air containing 21 mass% O_2, 70.5 mass% N_2 and 8.5 mass% H_2O vapor. The reactants velocities at the anode and cathode inlets were fixed at 2.2 and 4.5 m/s, respectively. The cell voltage was fixed at a value of 0.6 V.

Fig. 2 shows the variation of average current density with the permeability of the metal foam used in the flow-field of the bipolar/end plate. As was expected, the performance of the cell increased steadily when the permeability was decreased. At very low permeability values, comparable to that of the electrodes, the increase in performance starts to flatten up. So it is clear that lower permeability values of the flow-field will enhance the fuel cell performance. As

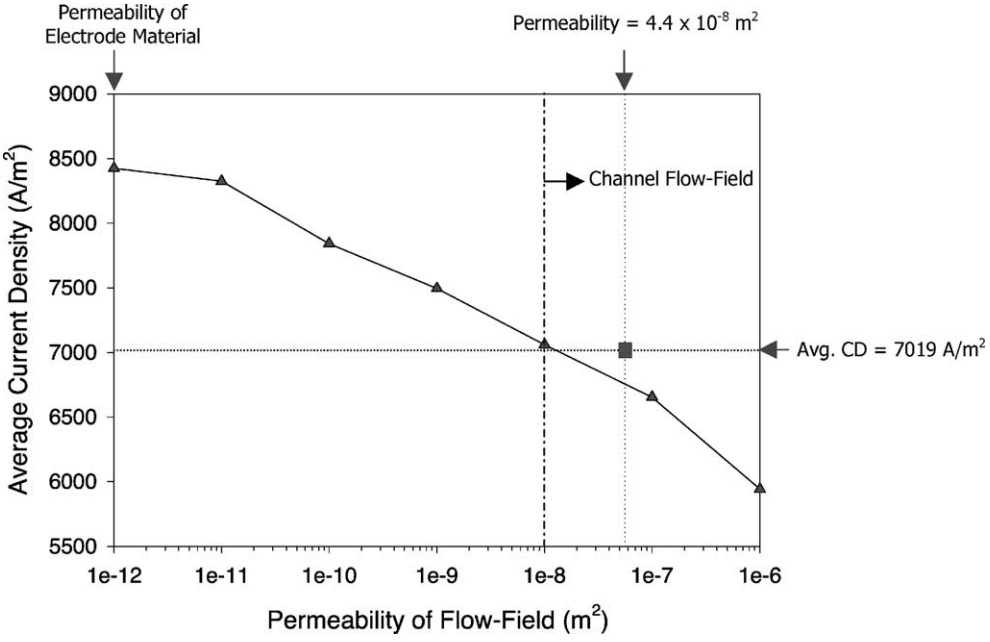

Fig. 2. Variation of average current density with the permeability levels of the metal foam in the flow-field of the bipolar/end plates.

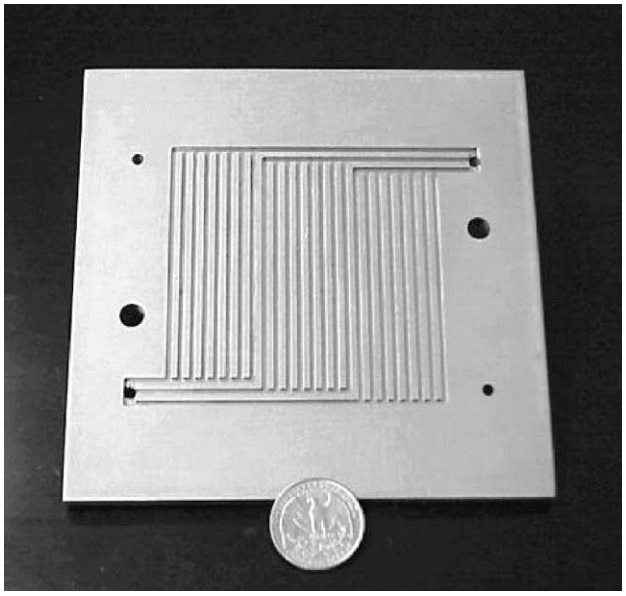

Fig. 3. Picture of SS-316 bipolar plate with multi-parallel flow-field design, designed and developed at The University of Alabama [4].

already stated, lower values of permeability of the flow-field are difficult to achieve in the machined channeled flow-field. Consequently, the use of metal foam will be preferred. We did the simulations for multi-parallel design with channel in the flow-field (Fig. 3), to compare its performance with that of the porous metal foam flow-field. The equivalent permeability of this channel design was calculated using the expression [5]:

$$\alpha = \frac{N_c(\Delta z/2)^2 \Delta x_c}{L} \times \left[\frac{1}{3} - \left(\frac{64}{\pi^5}\right)\frac{\Delta z}{\Delta x_c}\sum_{n,\text{odd}}^{\infty}\frac{1}{n^5}\tanh\left(\frac{n\pi\Delta x_c}{2\Delta z}\right)\right] \quad (37)$$

where N_c is the number of channels, Δx_c the channel width, Δz the thickness of the channels and L the length of the channel. The value of the equivalent permeability for the multi-parallel flow-field channel design ($N_c = 24$, $\Delta x_c = 0.0625$ in., $\Delta z = 0.0625$ in., $L = 3$ in.) was 4.4×10^{-8} m^2. The average current density obtained for this case was 7019 A/m^2 (square mark in Fig. 2). The value for average current density using the metal foam, but the same permeability value was 6794 A/m^2. It may be noticed that the average current density for the metal foam is slightly lower that that for the channel design with same permeability. However, the permeability of the metal foam can be decreased to improve the fuel cell performance. But on the other hand, it is practically difficult to reduce the permeability of the channel flow-field below a certain level (typically 10^{-8} m^2), due to difficulty in machining thinner channels. Also it is important to note that with use of metal foam, a more uniform distribution of current density is obtained. Figs. 4 and 5 shows that distribution of local current density on the electrode–membrane interface for the channel and metal foam type flow-field. It is clearly seen

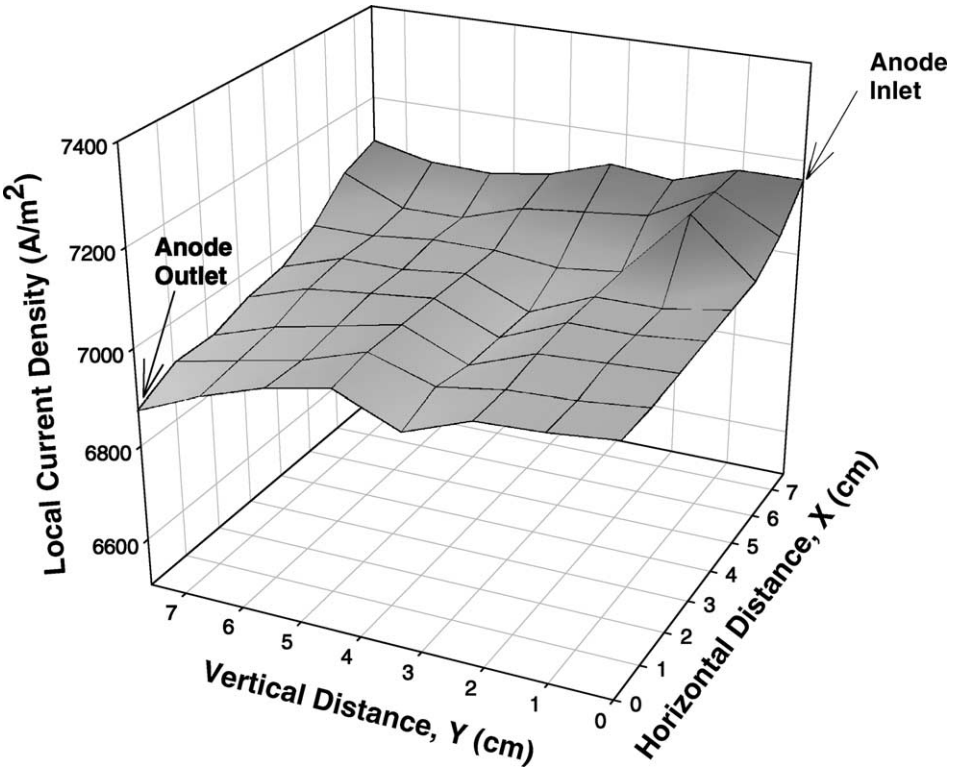

Fig. 4. Distribution of local current density on the electrode–membrane interface for the multi-parallel flow-field channel design. Average current density = 7019 A/m^2.

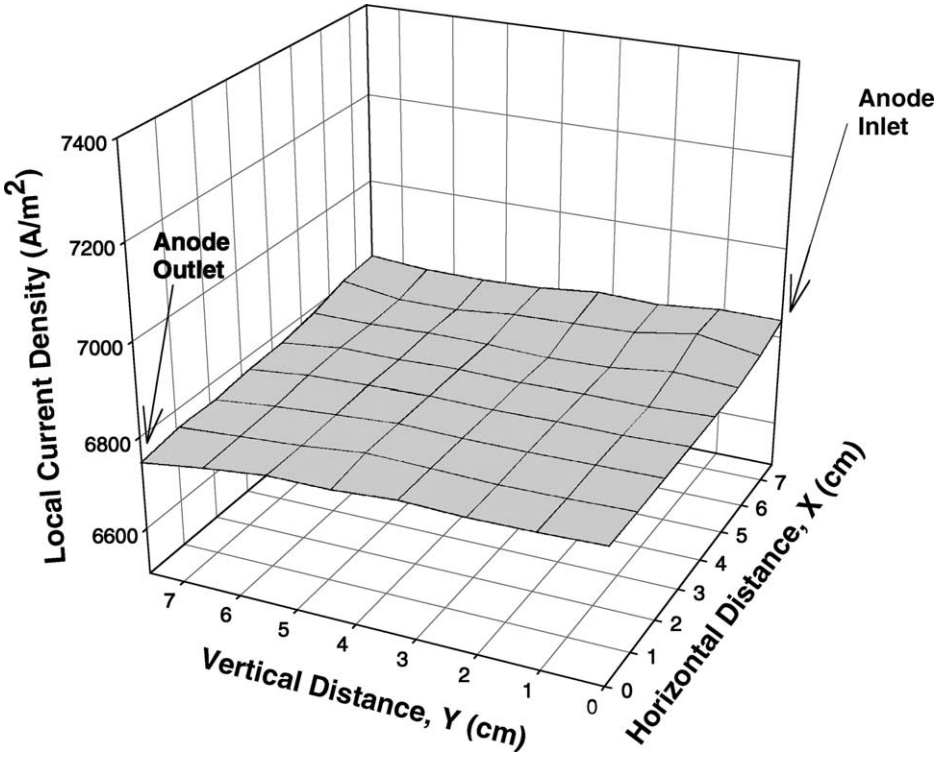

Fig. 5. Distribution of local current density on the electrode–membrane interface with metal foam in the flow-field of the bipolar/end plates. Average current density = 6794 A/m^2.

that in case of using metal foam a more uniform distribution of local current density is observed.

4. Conclusions

A unified, three-dimensional, steady-state numerical mass-transfer single cell model for polymer electrolyte membrane fuel cell (PEMFC) with metal foam in the flow-field was developed. Simulations were performed using various permeability levels of the metal foam ranging from 10^{-6} to 10^{-12} m^2. It was observed that the average current density increases from 5943 to 8425 A/m^2 when the permeability of the metal foam flow-field was decreased from 10^{-6} to 10^{-12} m^2. However, the rate of increase of current density decreases when the permeability values were decreased to the order of that of the electrode permeability ($\sim 10^{-12}$ m^2). Further, with the use of metal foam, a more uniform distribution of local current density was obtained compared to that for the channel flow-field design. The use of metal foam in the flow-field of the bipolar plate with proper permeability values will surely enhance the performance of the fuel cell.

Acknowledgements

The authors are grateful for the support of this work by Center of Advanced Vehicle Technologies (CAVT) at The University of Alabama, which is funded by United States Department of Transport (US DOT) Grant No.: DTFH61-91-X-00007.

References

[1] Review of the Research Program of the Partnership for a New Generation of Vehicles (PNGV), Sixth Report, Report PNGV/2000, National Academy Press, Washington, DC, 2000.
[2] Fuel cell Handbook, 5th ed., EG & G Services, Parsons Inc., US Department of Energy, Office of Fossil Energy, National Energy Technology Laboratory, West Virginia, 2000, pp. 1.1–1.37, 2.4–2.8.
[3] NECAR 4: The Alternative Daimler Chrysler, Corporate Communications, Stuttgart, 1999.
[4] A. Kumar, R.G. Reddy, in: D. Chandra, R.G. Bautista (Eds.), Fundamentals of Advanced Materials for Energy Conversion, TMS, 2002, pp. 41–53.
[5] E. Hontanon, M.J. Escudero, C. Bautista, P.L. Garcia-Ybarra, L. Daza, J. Power Sources 86 (2001) 363–368.
[6] D. Thirumalai, R.E. White, J. Electrochem. Soc. 144 (1997) 1717–1723.
[7] A. Kumar, R.G. Reddy, Effect of Channel Dimensions and Shape in the Flow-Field Distributor on the Performance of the Polymer Electrolyte Membrane Fuel Cells, J. Power Sources, 2002, in press.
[8] S. Dutta, S. Shimpalee, J.W. Van Zee, Intl. J. Heat Mass Transfer 44 (2001) 2029–2042.
[9] User Guide Documentation-Fluent 5.5 Computational Fluid Dynamics Software, 2002, Lebanon, New Hampshire. Retrieved from http://www.fluent.com on May 28, 2002.
[10] R.F. Mann et al., J. Power Sources 86 (2000) 173–180.

[11] D.R. Hodgson, B. May, P.L. Adcock, D.P. Davies, J. Power Sources 96 (2001) 233–235.
[12] T.E. Springer, M.S. Wilson, S. Gottesfeld, J. Electrochem. Soc. 140 (1993) 3513–3544.
[13] T.V. Nguyen, R.E. White, J. Electrochem. Soc. 140 (1993) 2178–2186.
[14] J.S. Yi, T.V. Nguyen, J. Electrochem. Soc. 145 (1998) 1149–1159.
[15] J.S. Yi, T.V. Nguyen, in: Proceedings of the First International Symposium on Proton Conducting Membrane Fuel Cells, The Electrochemical Society Inc., Pennington, NJ, vols. 23–95, 1995, pp. 66–75.